Numerical simulations of spray flames

By R. Kurose, O. Desjardins, M. Nakamura†, F. Akamatsu† AND H. Pitsch

1. Motivation and objectives

Spray combustion is utilized in a number of engineering applications such as energy conversion and propulsion devices. It is, therefore, necessary to precisely predict the spray combustion behavior in designing and operating the equipment. However, since spray combustion is a complex phenomenon in which dispersion of the liquid fuel droplets, evaporation, and chemical reaction of the fuel vapor with oxidizer take place interactively at the same time, the underlying physics governing these processes has not been well understood.

Direct numerical simulations (DNS) directly solve conservation equations for the carrier gaseous phase and Lagrangian equations for dispersed droplet dynamics and can be used for discussing the detailed spray combustion mechanism. However, few of such studies have been done even for low Reynolds numbers and simple geometries, because such simulations can be quite expensive.

Likewise, although large-eddy simulations (LES) are becoming a standard tool to study and predict single-phase gaseous combustion fields (e.g., Huang *et al.* 2003; Pierce & Moin 2004; Selle *et al.* 2004), the number of LES studies of two-phase combustion fields is very limited. Recently, Kurose & Makino (2003) applied LES to a turbulent jet flame of solid fuel and investigated the interactions among the dispersion, evaporation and combustion of solid-fuel particles. Ham *et al.* (2003) also performed LES of a spray combustion field in a realistic gas turbine combustor. The small number of papers on LES of two-phase combustion is attributed not only to the high computational cost, but also to the lack of experimental data for the validation.

In LES modeling of gaseous fuel combustion, the widely-used flamelet models (Peters 1984, 2000) have been extensively validated in different formulations, such as the steady-flamelet model (Cook *et al.* 1997), the unsteady-flamelet models (Pitsch & Steiner 2000; Pitsch 2002), and the flamelet/progress-variable approach (Pierce & Moin 2004). However, for spray combustion, the mixture fraction, which characterizes the mixing field, is not a conserved scalar anymore. Evaporation changes the mixing field, and especially the scalar dissipation rate. A proper formulation accounting for all the effects has not yet been developed. In addition, the validity of the standard approach for representing a group of droplets so called parcel to reduce the computational cost should be carefully studied, since the use of the parcels may deteriorate the numerical accuracy. In fact, it was demonstrated that the spray combustion behavior varies with the number of parcels (Nakamura *et al.* 2004), and it is expected that this phenomenon can be explained in terms of the droplet group combustion theory (Chiu & Liu 1977; Chiu *et al.* 1982).

The purpose of this work is twofold. First, the spray combustion behavior is studied by a two-dimensional DNS of spray flames formed in a laminar counterflow. The droplet group combustion theory (Chiu & Liu 1977; Chiu *et al.* 1982) is discussed in detail. The

† Osaka University

second aim of this work is to apply LES with the flamelet/progress-variable approach to a spray jet flame and validate the technique. Qualitative results are presented and compared with experimental observations.

2. Two-dimensional direct numerical simulation of spray flames stabilized in a laminar counterflow

2.1. *Field description and numerical method*

The computational setup for DNS of a spray flame in a laminar counter flow is designed to match the experiment of Hwang *et al.* (2000), and the numerical details are described in Nakamura *et al.* (2004). The computational domain analyzed in this study is shown in Figure 1. The dimensions are 20 mm × 40 mm. There are two burner ports with the widths of 20 mm on both the upper and lower sides, and the separation distance between the ports is 20 mm. The origin of the calculation domain is located at the center of the upper burner port. From the upper port of -10 $\leq y \leq$ 10 mm, atmospheric air (T = 300K, P = 0.1013 MPa, and oxygen mass fraction Y_{O_2} = 0.2357) is issued at a velocity of 0.4 m/s. From the lower port, a premixture of atmospheric air and n-decane ($C_{10}H_{22}$) vapor (equivalence ratio, ϕ = 0.6) is issued in the region of -3 $\leq y \leq$ 3 mm, and atmospheric air is issued in the region of -10 $\leq y \leq$ -3 mm and 3 $\leq y \leq$ 10 mm at the velocity of 0.4 m/s. The stretch ratio of the laminar counterflow is 40 1/s. The n-decane ($C_{10}H_{22}$) spray is injected from the upper port in the range of -3 $\leq y \leq$ 3 mm at the velocity of 0.4 m/s.

Gaseous species considered in the calculations are O_2, N_2, CO_2, H_2O, and $C_{10}H_{22}$, and their transport properties and thermodynamic data are obtained from CHEMKIN (Kee *et al.* 1986, 1989). Properties of liquid n-decane are obtained from Reid *et al.* (1977). The governing equations considered for the gaseous phase (mass, momentum, energy and species mass) are discretized and solved by the finite volume method using the SIMPLE algorithm (Patankar 1980). Dispersed droplets are tracked in a Lagrangian manner. It is assumed that the density of the droplets is much larger than that of the continuous phase such that only drag and gravity are significant. The effect of fluid shear on fluid force acting on the droplets (Saffman 1965; Kurose & Komori 1999), droplet breakup and collision, and dense particulate effects (Ham *et al.* 2003; Apte *et al.* 2003) are neglected. It is well known that the drag is reduced by evaporation. This effect is taken into account using the method by Kurose *et al.* (2003). Mass, heat and momentum interchanges between the carrier gas and dispersed droplet phases are calculated by the PSI-Cell model (Crowe *et al.* 1977). For the droplet evaporation, a non-equilibrium Langmuir-Knudsen evaporation model is employed (Miller & Bellan 1999).

Although the time-averaged equivalence ratio of the spray, ϕ_l, was 0.42 in the experiment (Hwang *et al.* 2000; Nakamura *et al.* 2004), this value was considered to vary periodically with time due to the unsteadiness of the fuel injection system. Hence, the computations are performed for four different spray equivalence ratios of ϕ_l = 0.21, 0.42, 0.84 and 1.26. The initial droplet size distribution is the same as that obtained by the PDA (phase Dopper anemometer) measurement (Figure 2), and the initial position of each droplet is determined randomly. The calculation domain (0 $\leq x \leq$ 20 mm, -20 $\leq y \leq$ 20 mm) is divided into 200 × 400 equally spaced computational cells in x and y directions, respectively, which generates the actual control volume size of 100 μm × 100 μm. The calculation time step is set at 0.1 ms.

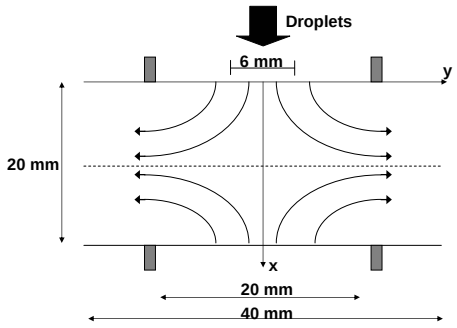

FIGURE 1. Computational domain for DNS of spray flames in a laminar counterflow.

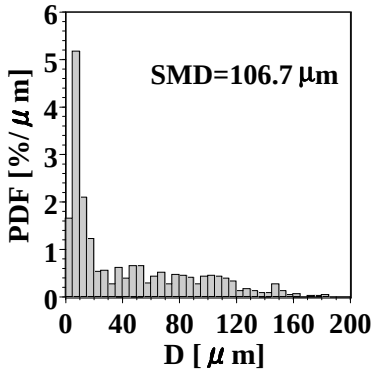

FIGURE 2. Initial droplet size distribution.

2.2. *Results and discussion*

Figure 3 shows the time-averaged axial (x direction) profiles of gaseous temperature, T, and axial velocity, u, respectively (at $y = 0$). The solid, dashed, dotted and dash-doted lines show the results of spray flames for $\phi_l = 0.21$, 0.42, 0.84 and 1.26, respectively. In general, as ϕ_l increases, the high T region expands, which is expected because the heat of reaction of the added spray increases with increasing ϕ_l. However, in the upper part of the high T region of $0.3 \leq x/L_x \leq 0.55$ (L_x is the separation difference between the ports), the value of T tends to decrease for high spray equivalence ratios of $\phi_l = 0.84$ and 1.26. It is also observed that, in accordance with the T profile, the difference in u between $\phi_l = 0.84$ and 1.26 is less for the upper region ($x/L_x \approx 0.4$) than that for the lower region ($x/L_x \approx 0.75$).

To investigate the spray combustion behavior in detail and clarify the reason why the gaseous temperature decreases for high spray equivalence ratio in the region of $0.3 \leq x/L_x \leq 0.55$, the instantaneous combustion fields for $\phi_l = 0.21$, 0.42, 0.84 and 1.26 are shown in Figure 4. Gas phase temperature, T, combustion reaction rate, R_F, and gas phase equivalence ratio, ϕ, are illustrated, and the droplet location is superimposed on each figure. The high combustion reaction rate around $x/L_x = 0.75$ in the figure of R_F (indicated by arrow F) is due to the flame of the premixed gases supplied from the lower port. The photograph of the flame obtained from the experiment, which, as will be explained later, is considered to correspond to the adjacent numerical condition, is also shown (Nakamura *et al.* 2004). It is found that, with increasing ϕ_l, the number of droplet entering the high temperature region increases, and the combustion behavior changes drastically. That is, while the droplets for low spray equivalence ratio of $\phi_l = 0.21$ monotonically evaporate and burn individually, those for higher spray equivalence ratio experience two different combustion zones, as shown in the distributions of R_F and ϕ. Firstly, for the high spray-equivalence-ratio cases of $\phi_l = 0.84$ and 1.26, the high R_F zone appears around the front surface of the high T region at $x/L_x = 0.35$ (indicated by arrow C). Although the droplets continuously evaporate even in the upstream region of

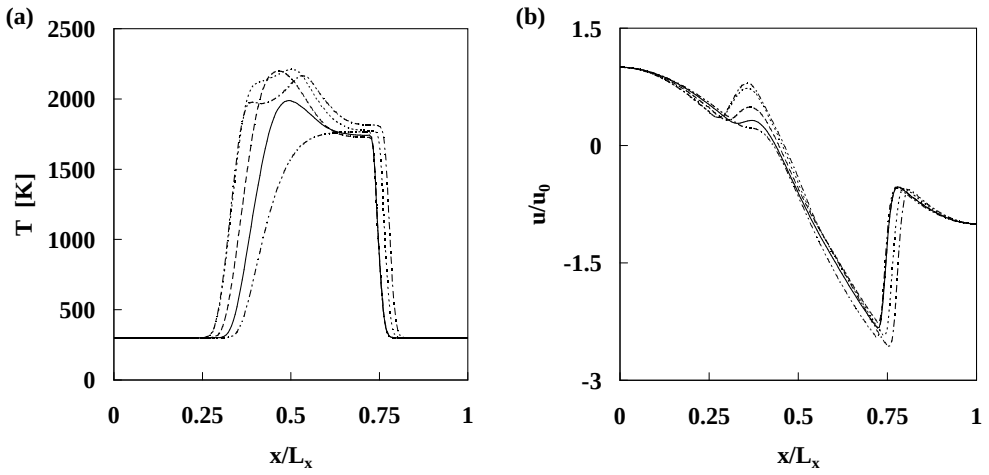

FIGURE 3. Time-averaged axial profiles of gaseous temperature and axial velocity: (a) temperature, T; (b) axial velocity, u; solid line, $\phi_l = 0.21$; dashed line, $\phi_l = 0.42$; dotted line, $\phi_l = 0.84$; dash-dotted line, $\phi_l = 1.26$; dash-double-dotted line, gaseous flame.

this zone (see the figure of ϕ), combustion does not occur until the fuel vapor reaches this zone. It can be said that a "premixed-like combustion" takes place in this zone, since the fuel vapor mixes with air before reaction starts. Subsequently, in the downstream region of $0.35 \leq x/L_x \leq 0.5$ (between arrows C and E), there appears a "diffusion-like combustion" zone, where the evaporation and combustion of the residual droplets penetrating the "premixed-like combustion" zone takes place at the same time.

Furthermore, this "diffusion-like combustion" is apparently divided into two different combustion types. The residual droplets in the high T region evaporate and burn individually in the upper region ($0.35 \leq x/L_x \leq 0.4$ (between arrows C and D)), but burn as clusters of some droplets in the lower region ($0.4 \leq x/L_x \leq 0.5$ (between arrows D and E)). The difference in the combustion type can be explained by Figure 5, which shows the instantaneous axial profiles of gaseous temperature, T, mass fraction of O_2 and $C_{10}H_{22}$, Y_{O_2} and $Y_{C_{10}H_{22}}$, and combustion reaction rate, R_F, on the A and B section in Figure 4. The oxygen is abundant in the upper region of $0.35 \leq x/L_x \leq 0.4$, but almost zero in the lower region of $0.4 \leq x/L_x \leq 0.5$. Therefore, the fuel vapor generated in the high T region rapidly reacts with the oxygen and is consumed in the former condition, whereas it is not consumed in the latter condition. Consequently, the high fuel vapor lumps containing some droplets burn from the outer surface, where the oxygen is abundant.

This phenomenon, in which the droplets burn as a cluster, is known as droplet group combustion. According to Chiu & Liu (1977) and Chiu *et al.* (1982), there are four modes in spray flames, i.e., (1) single droplet combustion mode, in which droplets burn as a single droplet, (2) internal group combustion mode, in which group flames appear inside the droplet group (droplets inside the group flame only just evaporate and droplets outside the group flame burn as a single droplet), (3) external group combustion mode, in which the group flame encloses the whole droplet group, and (4) external sheath combustion mode, in which a non-evaporation region (low temperature region) is found inside the evaporation region in the droplet group. These modes change from the single droplet

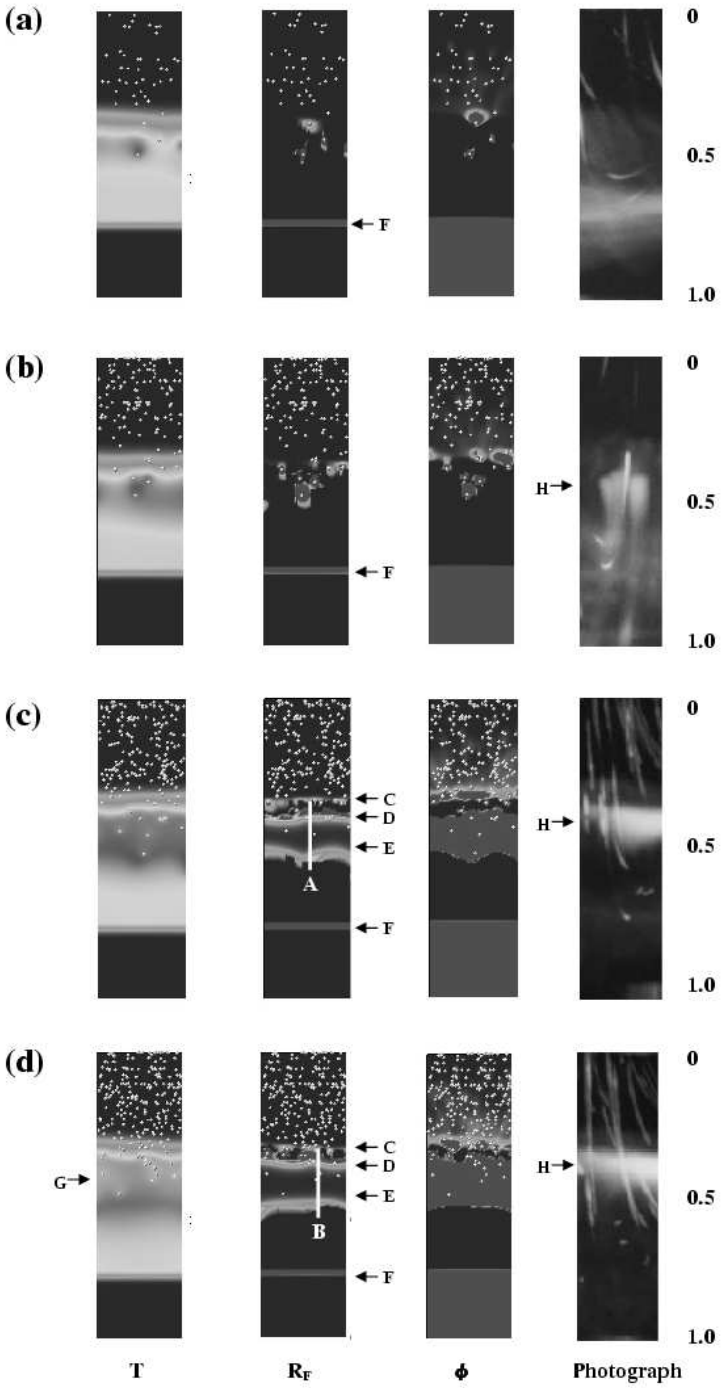

FIGURE 4. Instantaneous distributions of gaseous temperature, T, combustion reaction rate, R_F, gaseous equivalence ratio, ϕ, and photograph in the central region of counterflow ($-0.15 \leq y/L_x \leq 0.15$): (a) $\phi_l = 0.21$; (b) $\phi_l = 0.42$; (c) $\phi_l = 0.84$; (d) $\phi_l = 1.26$.

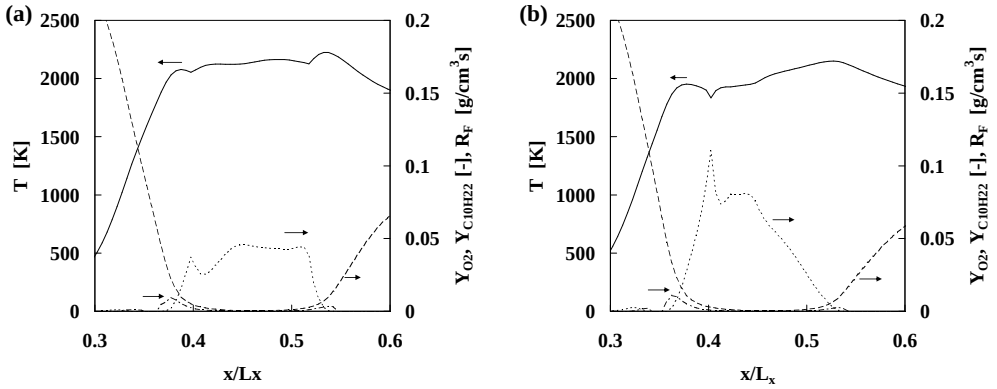

FIGURE 5. Instantaneous profiles of gaseous temperature, T, mass fractions of O_2 and $C_{10}H_{22}$, Y_{O_2} and $Y_{C_{10}H_{22}}$, and combustion reaction rate, R_F, on the A and B section in Figure 4: (a) $\phi_l = 0.84$; (b) $\phi_l = 1.26$; solid line, T; dashed line, Y_{O_2}; dotted line, $Y_{C_{10}H_{22}}$; dash-dotted line, R_F.

combustion mode to the external sheath combustion mode, as the group combustion number, G, increases.

In Figure 4, for the highest spray-equivalence-ratio cases of $\phi_l = 1.26$, low temperature lumps containing some droplets appear (see arrow G in the temperature profile in Figure 5). This is becasue that this combustion belongs to the external sheath combustion mode. The decrease of the gaseous temperature for high spray equivalence ratios of $\phi_l = 0.84$ and 1.26 in the upper part of the high T region of $0.3 \leq x/L_x \leq 0.55$, as shown before, is considered to be caused by the group combustion behavior. The reason why the gaseous temperature decreases in the droplet group is due to the heat exchange between droplets and gaseous phase, which is referred to as the evaporative cooling effect. The temperature of droplets is much lower than that of the gaseous phase. Moreover, as the evaporation of droplets proceeds, the heat of vaporization reduces the droplet temperature. This low gaseous temperature leads to the low reaction rates. Thus, droplet group combustion, which tends to appear in the regions of high droplet number density and low oxygen concentration, delays the combustion reactions.

As mentioned earlier, although the time-averaged equivalence ratio of the spray, ϕ_l, was 0.42 in the experiment, this value was considered to vary with time. Hence, the flame photograph, which seems to correspond to each numerical condition, is selected in Figure 4. In the photographs, blue and luminous flames indicate premixed and diffusion combustion (the flames are shown in white and the luminous flames are indicated by arrows H), respectively, since the lumination originates from soot radiation, which is generated under very rich conditions, such as those encountered in diffusion flames. It seems that the computed results generally agree with the experimental observations. For the high spray equivalence ratios of $\phi_l = 0.84$ and 1.26, the sizes and positions of the computed group combustion flames correspond to those of the luminous flames.

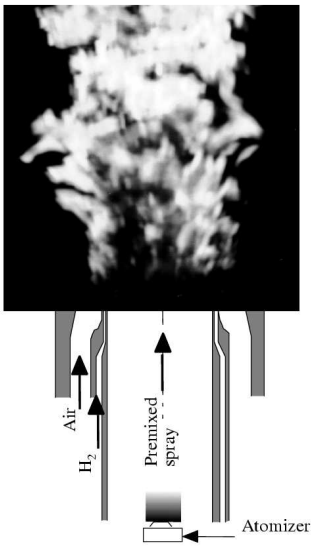

FIGURE 6. Premixed-spray jet flame (Akamatsu *et al.* 1996).

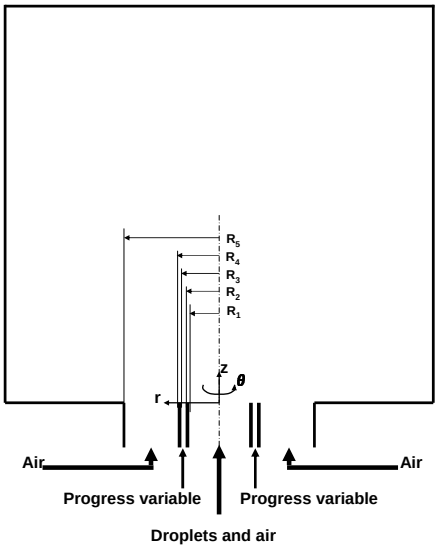

FIGURE 7. Computational domain for LES of a spray jet flame.

3. Large-eddy simulation of a spray jet flame

3.1. *Field description and numerical method*

The spray jet flame considered here has first been experimentally investigated by Nakabe *et al.* (1988, 1991, 1994) and the detailed flame behavior has been studied by Akamatsu *et al.* (1996, 1997) using several kinds of optical measurement techniques. The spray jet flame is a non-swirling piloted jet flame stabilized in a two-phase stream with minimum slip between gas and droplets, for which a long mixing length from a spray atomizer to burner outlet is given (Figure 6). It is called premixed-spray jet flame. A liquid fuel atomized by an air-blast atomizer placed upstream is issued in air from the central port of the annular pilot burner. This premixed-spray jet flame has the advantage that complicated phenomena such as dense particle flow effects and spray breakup, collision, and deformation (e.g., Ham *et al.* 2003; Apte *et al.* 2003) can be neglected in the computations.

The computations performed in this study are designed to match the experimental setup (Akamatsu *et al.* 1996, 1997). The computational domain is shown in Figure 7. The computational domain normalized by the burner radius (R_5) is -1 $\leq$ z $\leq$ 10, 0 $\leq$ r $\leq$ 6 and 0 $\leq \theta \leq 2\pi$ in the axial, radius and azimuthal directions (R_1 = 26.35 mm, R_2 = 27.35 mm, R_3 = 28.35 mm, R_4 = 29.35 mm, R_5 = 40.45 mm). In the experiments, kerosene is used as the liquid fuel, hydrogen is supplied from the annular pilot burner, and air is provided from the surrounding annulus to suppress the expansion of the stream lines. In this preliminary test, however, n-heptane is assumed as the liquid fuel, and the annular pilot burner to ignite and stabilize the spray flame is modeled by a stream of hot combustion products. The nominal bulk velocity of the central and surrounding air is 5.5 m/s.

The numerical procedure is essentially the same as that of Pierce and Moin (2001). A structured grid in cylindrical coordinates is used. The primary breakup of the liquid jet is not computed. Instead, the initial droplet size distribution obtained by the PDA measurement is used. The simplified model by Oefelein (1997) is used for droplet evaporation.

The size of the grid is $272 \times 128 \times 96$ nodes in the axial, radial, and azimuthal directions, respectively, and the grid is refined near the solid boundaries. The parcels representing about 20 droplets are tracked, which yields around 0.7 million parcels in the domain.

3.2. *Results and discussion*

Figures 8 and 9 show the instantaneous distributions of mixture fraction and product mass fraction together with the droplet distribution. Only mixture fractions and product mass fractions larger than 0.05 are shown. The spray jet flame is found to be stabilized by the product mass fraction issued from the annular pilot burner. For both the mixture fraction and product mass fraction, high concentration regions are observed around the spray jet, which means that combustion proceeds from the outside of the spray jet. Although not apparent only from these figures, in the upstream region near the burner, most of the droplets evaporate on the edge of the spray jet and hardly penetrate into the outer high product mass fraction area. In the downstream region of the spray jet, on the other hand, some droplets are found to separate from the main spray jet and move into the high product mass fraction area as clusters, as shown in Figure 10. A similar behavior was observed in the previous experiment by Tsushima *et al.* (see Figure 11). The numerical results also illustrate that, for the droplet cluster in the high product mass fraction area, the high temperature droplets tend to cover the low temperature droplets. This trend seems to correspond to the earlier described mode (3) or (4) , which suggests that the present LES is capable of capturing the droplet group combustion behavior. However, quantitative validation using an improved droplet evaporation model and chemical mechanism for a better kerosene surrogate would be essential to fully validate the technique.

4. Conclusions and future work

This paper presented the detailed behavior of spray flames by analysing 2-D DNS data for burning liquid fuel spray in a laminar counterflow. The droplet group combustion model (Chiu & Liu 1977) was explicitly demonstrated. It was also verified that the droplet group combustion tends to appear in the region of high droplet number density and low oxygen concentration and that it delays evaporation and combustion of the fuel droplets.

LES with the flamelet/progress-variable approach was applied to a spray jet flame, and preliminary test case results were shown. The spray jet flame was stabilized by supplying the progress variable from the annular pilot burner, and corresponding the experimental observations, the group combustion-like behavior was observed.

Future work will focus on the validation study for the LES technique of spray jet flames. First of all, an improved droplet evaporation model and a chemical mechanism for a kerosene surrogate will be implemented in the LES code. Our detailed experimental data for the premixed-spray jet flame (e.g. gaseous velocity, temperature, main species concentrations, droplet size, and droplet number density) will allow us to understand

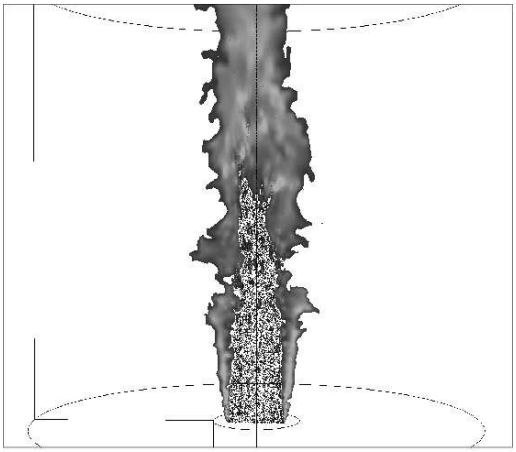

FIGURE 8. Instantaneous distributions of mixture fraction and droplets.

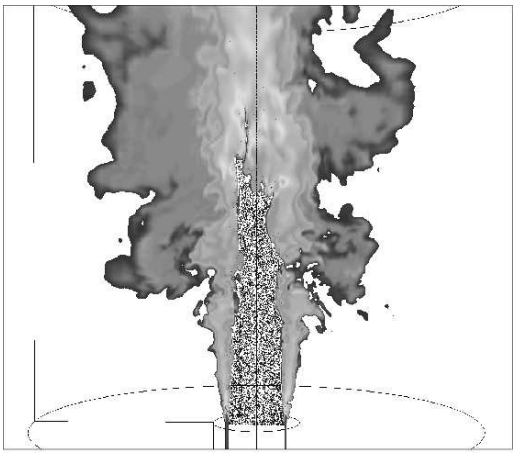

FIGURE 9. Instantaneous distributions of product mass fraction and droplets.

the accuracy of the existing models associated with droplet evaporation and combustion, and to develop improved models.

Acknowledgments

The authors are grateful to Drs. Sourabh Apte and Scott Martin for many helpful discussions and their comments on this manuscript. They also thank to Prof. Masashi Katsuki of Osaka University for many useful discussions. RK would like to thank Prof. Parviz Moin for providing a part of his expenses during his stay at Stanford through the Center for Turbulence Research Senior Visiting Fellow Program.

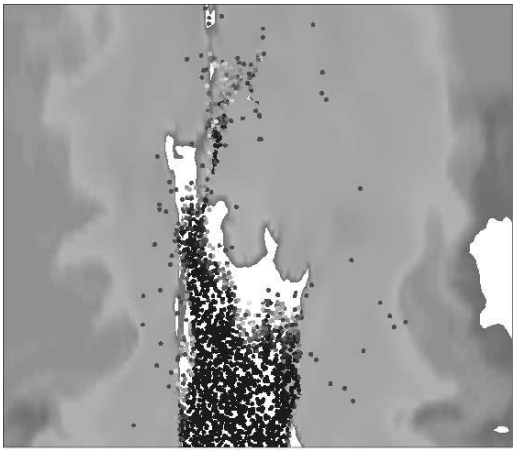

FIGURE 10. Magnified instantaneous distributions of product mass fraction and droplets.

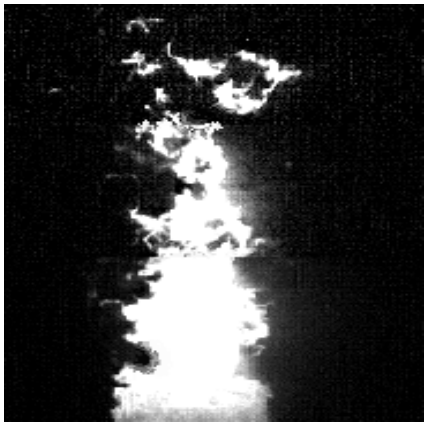

FIGURE 11. Droplet distribution obtained by experiment (Tsushima *et al.* 1998).

REFERENCES

AKAMATSU, F., MIZUTANI, Y., KATSUKI, M., TSUSHIMA, S. & CHO, Y. D. 1996 Measurement of local group combustion number of droplet clusters in a premixed spray stream. *Proc. of the Combustion Institute* **26**, 1723-1729.

AKAMATSU, F., MIZUTANI, Y., KATSUKI, M., TSUSHIMA, S., CHO, Y. D. & NAKABE, K. 1997 Group combustion behavior of droplets in a premixed-spray flame. *Atomization and Sprays* **7**, 199-218.

APTE, S. V., GOROKHOVSKI, M. & MOIN, P. 2003 LES of atomizing spray with stochastic modeling of secondary breakup. *Int. J. Multiphase Flow* **29**, 1503-1522.

CHIU, H. H. & LIU, T. M. 1977 Group combustion of liquid droplets. *Combust. Sci. Tech.* **17**, 127-142.

CHIU, H. H., KIM, H. Y. & CROKE, E. J. 1982 International group combustion of liquid droplets. *Proc. of the Combustion Institute* **19**, 971-980.

COOK, A. W., RILEY, J. J. & KOSÁLY, G. 1997 A laminar flamelet approach to subgrid-scale chemistry in turbulent flow. *Combust. Flame* **109**, 332-341.

CROWE, C. T., SHARMA M. P. & STOCK, D. E. 1977 The particle-source-in cell (PSI-CELL) model for gas-droplet flows. *Trans. ASME, J. of Fluids Eng.* **99**, 325-332.

HAM, F., APTE, S.V., IACCARINO, G., WU, X., HERRMANN, S., CONSTANTINESCU, G., MAHESH, K. & MOIN, P. 2003 Unstructured LES of reacting multiphase flows in realistic gas turbine combustors. *Annual Research Briefs-2003*, Center for Turbulence Research, NASA Ames/Stanford University, 139-160.

HUANG, Y., SUNG, H.-G., HSIEH, S.-Y. & YANG, Y. 2003 Large-eddy simulation of combustion dynamics of lean-premixed swirl-stabilized combustor. *J. Propul Power* **19**, 782-794.

HWANG, S.-M., SAITOH, H., TAKADA, S., AKAMATSU, F. & KATSUKI, M. 2000 Observation of Spray Flame Stabilized in a Laminar Counterflow Field. *Proc. of 38th Japanese Combustion Symposium*, 201-202, in Japanese.

KEE, R. J., DIXON-LEWIS, G., WARNATZ, J., COLTRIN, M. E. & MILLER, J. A. 1986 A fortran computer code package for the evaluation of gas-phase multicomponent transport properties. *SANDIA Report*, SAND86-8246.

KEE, R. J., RUPLEY, F. M. & MILLER, J. A. 1989 Chemkin-II: A fortran chemical kinetics package for the analysis of gas phase chemical kinetics. *SANDIA Report*, SAND89-8009B.

KUROSE, R. & KOMORI, S. 1999 Drag and lift forces on a rotating sphere in a linear shear flow. *J. Fluid Mech.* **384**, 183-206.

KUROSE, R., MAKINO, H., KOMORI, S., NAKAMURA, M., AKAMATSU, F. & KATSUKI, M. 2003 Effects of outflow from surface of sphere on drag, shear lift, and scalar diffusion. *Phys. Fluids* **15**, 2338-2351.

KUROSE, R. & MAKINO, H. 2003 Large eddy simulation of a solid-fuel jet flame. *Combust. Flame* **135**, 1-16.

MILLER, R. S. & BELLAN, J. 1999 Direct numerical simulation of a confined three-dimensional gas mixing layer with one evaporating hydrocarbon-droplet-laden stream. *J. Fluid Mech.* **384**, 293-338.

NAKABE, N., MIZUTANI, Y., HIRANO, T. & TANIMURA, S. 1988 Burning characteristics of premixed sprays and gas-liquid coburning mixtures. *Combust. Flame* **74**, 39-51.

NAKABE, N., MIZUTANI, Y., HIRANO, T. & FUJIOKA, H. 1991 An experimental study on detailed flame structure of liquid fuel sprays with and without gaseous fuel. *Combust. Flame* **84**, 3-14.

NAKABE, N., MIZUTANI, Y., AKAMATSU, F. & FUJIOKA, H. 1994 Observation of droplets group combustion in terms of simultaneous measurement of Mie-scattering and spectral luminosity of spray flame. *Atomization Sprays* **84**, 3-14.

NAKAMURA, M., AKAMATSU, F., KUROSE, R. & KATSUKI, M. 2004 Combustion mechanism of liquid fuel spray entering gaseous flame front, in preparation for submission.

OEFELEIN, J. C. 1997 Simulation and analysis of turbulent multiphase combustion processes at high pressures. Ph.D. Thesis, The Pennsylvania State University, University Park, Pa.

PATANKAR, S. V. 1980 *Numerical Heat Transfer and Fluid Flow*, McGraw-Hill.

PETERS, N. 1984 Laminar diffusion flamelet models in non-premixed turbulent combustion. *Prog. Energy Combust. Sci.* **10**, 319-339.

PETERS, N. 2000 *Turbulent Combustion*, Cambridge University Press.

PIERCE, C. D. & MOIN, P. 2001 Progress-variable approach for large-eddy simulation of turbulent combustion. *Mech. Eng. Dept. Rep.* **TF-80**, Stanford University.

PIERCE, C. D. & MOIN, P. 2004 Progress-variable approach for large-eddy simulation of non-premixed turbulent combustion. *J. Fluid Mech.* **504**, 73-97.

PITSCH, H. & STEINER, H. 2000 Large-eddy simulation of a turbulent piloted methane/air diffusion flame (Sandia flame D). *Phys. Fluids* **12**, 2541-2554.

PITSCH, H. 2002 Improved pollutant predictions in large-eddy simulations of turbulent non-premixed combustion by considering scalar dissipation rate fluctuations. *Proc. of the Combustion Institute* **29**, 1971-1978.

REID, R. C., PRAVSNITZ, J. M. & SHERWOOD, T. K. 1977 *The Properties of Gases and Liquids, third edition*, McGraw-Hill, New York.

SAFFMAN, P. G. 1965 The lift on a small sphere in a shear flow. *J. Fluid Mech.* **22**, 385-400, and 1968 Corrigendum **31**, 624.

SELLE, L., LARTIGUE, G., POINSOT, T., KOCH, R., SCHILDMACHER, K.-U., KREBS, W., PRADE, B., KAUFMANN, P. & VEYNANTE, D. 2004 Compressible large eddy simulation of turbulent combustion in complex geometry on unstructured meshes. *Combust. Flame* **137**, 489-505.

TSUSHIMA, S., SAITOH, H., AKAMATSU, F. & KATSUKI, M. 1998 Observation of combustion characteristics of droplet clusters in a premixed-spray flame by simultaneous monitoring of planar spray images and local chemiluminescence. *Proc. of the Combustion Institute* **27**, 1967-1974.